

pubs.acs.org/JACS Article

Selenomelanin: An Abiotic Selenium Analogue of Pheomelanin

Wei Cao, Naneki C. McCallum, Qing Zhe Ni, Weiyao Li, Hannah Boyce, Haochuan Mao, Xuhao Zhou, Hao Sun, Matthew P. Thompson, Claudia Battistella, Michael R. Wasielewski, Ali Dhinojwala, Matthew D. Shawkey,* Michael D. Burkart,* Zheng Wang,* and Nathan C. Gianneschi*



Cite This: J. Am. Chem. Soc. 2020, 142, 12802-12810



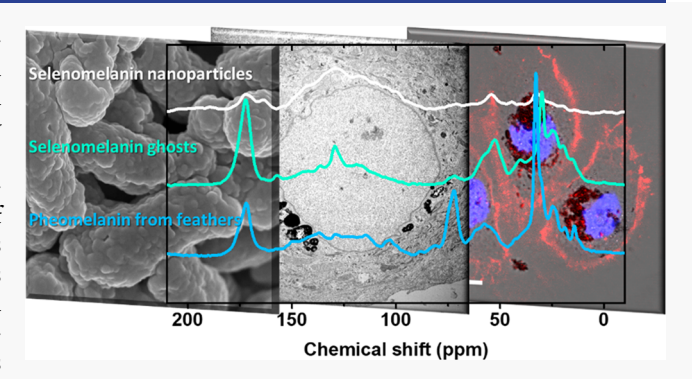
ACCESS

Metrics & More

Article Recommendations

s Supporting Information

ABSTRACT: Melanins are a family of heterogeneous biopolymers found ubiquitously across plant, animal, bacterial, and fungal kingdoms where they act variously as pigments and as radiation protection agents. There exist five multifunctional yet structurally and biosynthetically incompletely understood varieties of melanin: eumelanin, neuromelanin, pyomelanin, allomelanin, and pheomelanin. Although eumelanin and allomelanin have been the focus of most radiation protection studies to date, some research suggests that pheomelanin has a better absorption coefficient for X-rays than eumelanin. We reasoned that if a selenium enriched melanin existed, it would be a better X-ray protector than the sulfurcontaining pheomelanin because the X-ray absorption coefficient is proportional to the fourth power of the atomic number (Z).



Notably, selenium is an essential micronutrient, with the amino acid selenocysteine being genetically encoded in 25 natural human proteins. Therefore, we hypothesize that selenomelanin exists in nature, where it provides superior ionizing radiation protection to organisms compared to known melanins. Here we introduce this novel selenium analogue of pheomelanin through chemical and biosynthetic routes using selenocystine as a feedstock. The resulting selenomelanin is a structural mimic of pheomelanin. We found selenomelanin effectively prevented neonatal human epidermal keratinocytes (NHEK) from G2/M phase arrest under high-dose X-ray irradiation. Provocatively, this beneficial role of selenomelanin points to it as a sixth variety of yet to be discovered natural melanin.

INTRODUCTION

Natural and synthetic eumelanins have been studied for use as pigments, ^{1–5} structural color, ^{6,7} surface coatings, ⁸ dry/wet adhesives, ⁹ and free radical scavengers. ^{10–13} By contrast, pheomelanin is less studied, likely because it is structurally more complex than eumelanin and because pure pheomelanin is a rarity or is nonexistent, meaning it is never found without eumelanin in nature. ^{14,15} These features make its isolation prohibitively difficult. Pheomelanin is thought to be synthesized biologically from tyrosine and cysteine and contains benzothiazine subunits as evidenced by degradation studies and analysis of intermediates. ^{16,17} In addition to structural and pigmentation differences, ^{14,18,19} some research suggests that pheomelanin absorbs X-rays more efficiently compared to eumelanin. ²⁰

Unwanted exposure to ionizing radiation occurs during a vast array of common human activities from air travel, to X-ray diagnosis, to clinical radiation therapy, and in extreme cases such as nuclear reactor malfunction. Melanized organisms are found in high radiation exposure environments such as Chernobyl^{21,22} and in orbiting spacecraft. Melanin may act as a radioprotective shield by direct attenuation and/or by quenching of radical species. Therefore, the synthesis,

optimization, and study of melanins for use in ionizing-radiation protection for materials and living systems such as the protection of healthy tissue during radiation-based cancer treatments has been a research focus. Furthermore, given the increased interest in space travel (i.e., SpaceX, Virgin Galactic) and the role of nuclear power in a noncarbon-based electrical grid of the present and future, he lightweight multifunctional and radioprotective materials are needed.

Selenium compounds have been reported to protect animals against ionizing radiation, and inhibit apoptosis and inflammation in model studies. Selenium is an essential micronutrient. Indeed, the amino acid selenocysteine (Sec) is encoded by a UGA codon when the SECIS (SElenoCysteine Insertion Sequence) is present in the mRNA and is hence incorporated in 25 natural human proteins. This makes it

Received: May 22, 2020 Published: July 8, 2020





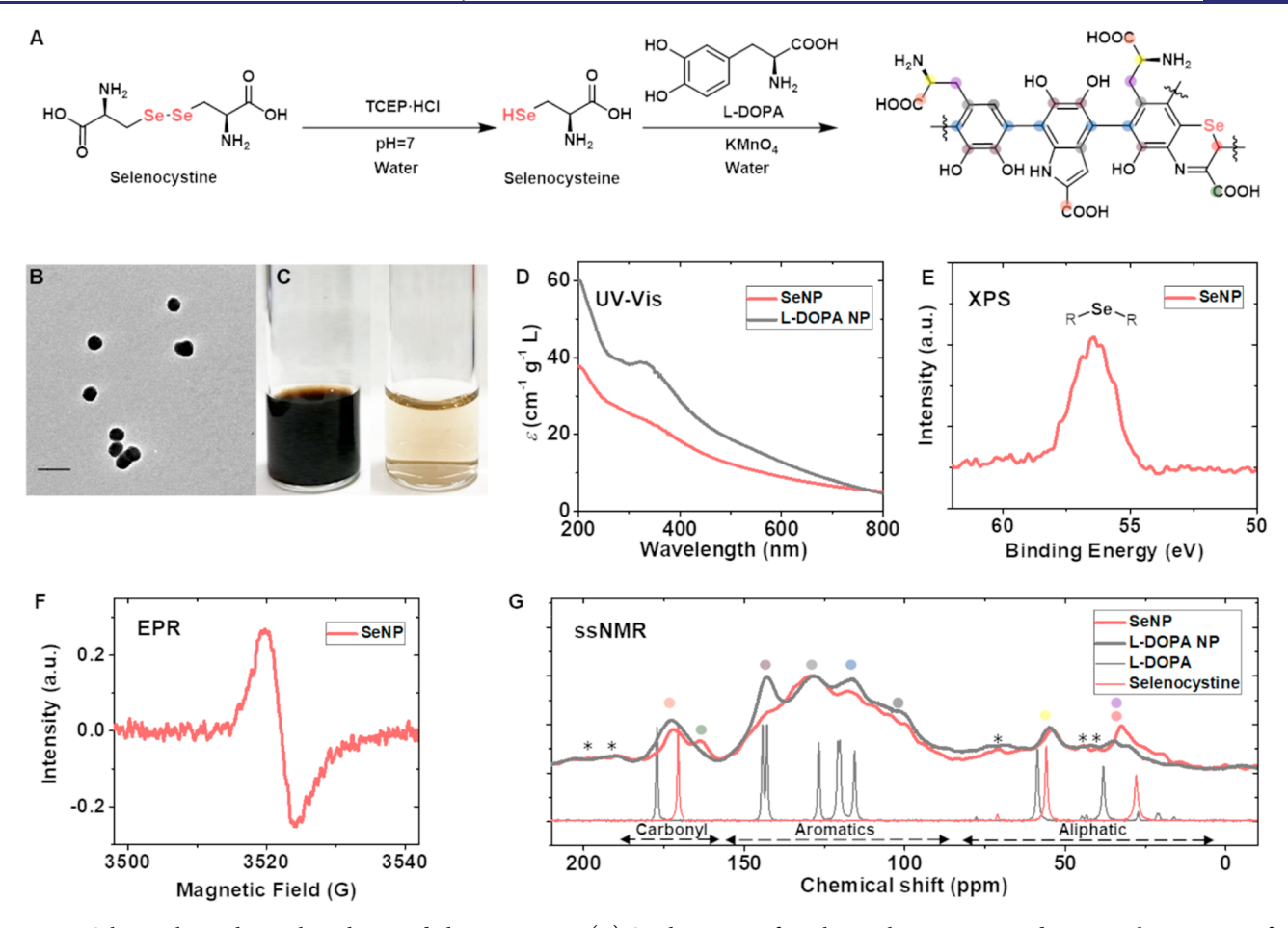


Figure 1. Selenomelanin chemical synthesis and characterization. (A) Synthetic route for selenomelanin NP *via* oxidative copolymerization of L-DOPA and selenocysteine. (B) Representative TEM image showing spherical SeNPs. Scale bar 200 nm. (C) Images of selenomelanin suspensions, 1 mg mL⁻¹ (left) and 0.02 mg mL⁻¹ (right). (D) Extinction coefficient of SeNP and L-DOPA NP. (E) XPS Se 3d spectrum. (F) EPR spectrum of SeNP. (G) ¹³C ssNMR spectra of SeNP overlaid with L-DOPA NP and monomers. Carbon assignments are listed adjacent to each main NMR peak based on the monomer peak comparison and previous literature. ²⁴ Colored dots in G correspond with the proposed structure in A. Spinning side bands of SeNP are labeled with asterisks (*).

a good candidate for examining selenium's role as a substitute in biomaterials that are known to naturally utilize cysteine. This is despite the difficulty of working with small molecule selenium compounds that have notorious odors, are redox sensitive, and undergo constant metathesis triggered by visible light.³³

We hypothesized that if a selenium enriched melanin existed in nature or could be generated in the laboratory, it would protect against X-rays better than the known sulfur-containing pheomelanin. Selenium is a heavier chalcogen than sulfur, with X-ray absorption proportional to $Z^{4,34}$ However, until selenomelanin is discovered naturally, a synthetic route must be devised to test its properties. The nucleophilic 1,6-addition of the cysteine thiol group to enzymatically generated dopaquinone is key for pheomelanin biosynthesis, ¹⁶ so it follows that incorporation of the more nucleophilic selenocysteine would yield a selenium version of pheomelanin.

Herein, we report the design, synthesis, and biosynthesis of selenomelanin. We demonstrate that synthetic selenomelanin contains benzoselenazine subunits, making it a direct analog to the known, naturally occurring, sulfur-containing pheomelanin. We prepare selenomelanin nanoparticles (SeNPs) which form perinuclear caps, or microparasols, in neonatal human epidermal keratinocyte (NHEK) cells, and significantly decrease cell cycle arrest following X-ray insult as compared

to synthetic pheomelanin or eumelanin. Furthermore, we show that radioprotective selenomelanin may be biosynthesized by bacteria fed selenocystine and L-3,4-dihydroxyphenylalanine (L-DOPA).

RESULTS AND DISCUSSION

Chemical Synthesis of Selenomelanin. The synthesis of selenomelanin was inspired by Lee and co-workers' synthesis of pheomelanin (Figure 1).35 A typical synthesis of selenomelanin involves the oxidation of L-DOPA in the presence of selenocysteine formed in situ by selenocystine reduction (Figure 1A). The reaction yields nanoparticles 160 nm in diameter (Figure 1B, Figure S1) with broadband absorption across the UV-visible region, as is typical for melanin (Figure 1C,D). Note that KMnO₄ has been previously used for melanin synthesis. 35,36 Under strongly acidic conditions (1 M H₂SO₄), 4 mM KMnO₄ can lead to decomposition of the polymer skeleton: a method used for HPLC-type analysis of these materials.^{37–39} However, in our experiments, the pH of the reaction was kept at approximately 7.0 and the KMnO₄ concentration was lower (1.4 mM). The extinction coefficient (ε) in the UV-Vis region is lower than that for nanoparticles made purely from L-DOPA (Figure 1D). Fourier-transform infrared (FTIR) spectroscopy of SeNPs

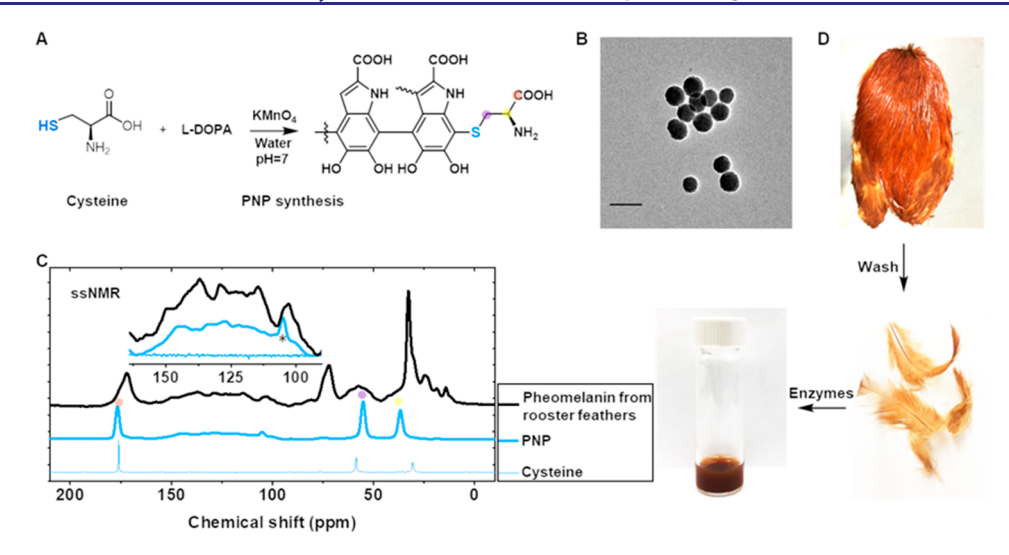


Figure 2. Pheomelanin nanoparticle (PNP) synthesis and comparative ssNMR with natural pheomelanin. (A) Synthetic route and proposed structure of PNP. (B) Representative TEM image of PNP. Scale bar 200 nm. (C) ¹³C ssNMR spectra indicate uncyclized cysteine in PNP. The PNP NMR spectrum was processed with 60 Hz Gaussian line broadening for clarity. Carbon assignments of PNP are listed adjacent to each NMR peak based on the monomer peak comparison. The aromatic peaks have low intensity, and assignment is impractical. Inset is the zoomed aromatic region of cysteine, PNP, and pheomelanin from bird feathers. The PNP spinning sideband is labeled with an asterisk (*). Rooster pheomelanin peaks at 172, 72, and 33 ppm were assigned to lipids. (D) Natural pheomelanin extraction from covert feathers of a Rhode Island red rooster shown in photography.

Table 1. Synthetic Melanin Nanoparticles Used in This Work

	Monomer	Oxidant	Size (R _h , nm)	ζ potential (mV)	Molar ratio of Sec/Cys to L-DOPAa	CD Signal ^b
SeNP	Selenocysteine, L-DOPA	$KMnO_4$	80	-20.3	0.44:1	_
PNP	Cysteine, L-DOPA	$KMnO_4$	89	-16.4	0.65:1	+
L-DOPA NP	L-DOPA	$KMnO_4$	90	-52.2	NA	_
^a The molar ratio was calculated from ICP-OES results. ^b CD spectra are shown in Figures S7 and S10.						

revealed absorption bands typical of melanins 40 at 3600–2400 cm $^{-1}$ (-OH, -COOH, -NH), 1715 cm $^{-1}$ (C=O), and 1616 cm $^{-1}$ ($-NH_2$, aromatic ring C=C) (Figure S2). X-ray photoelectron spectroscopy (XPS) confirmed the presence of the monoselenide (C-Se-C) functional group (Figure 1E, Figure S1). Electron paramagnetic resonance (EPR) spectroscopy (Figure 1F) indicates the material contains stable unpaired electrons with 1.12×10^{18} spins per gram (Figure S3), consistent with typical synthetic melanins.

The characterization of melanin is generally challenging due to its insolubility, hierarchical structure, and multiscale disorder (from covalent bonds, to redox states, to noncovalent interactions).2 Researchers have commonly relied on high performance liquid chromatography (HPLC) to separate components arising from degraded melanin. 17,20 However, solid-state nuclear magnetic resonance (ssNMR) offers key insights into the intact material.²⁴ Therefore, we employed comparative ssNMR analysis to study as prepared selenomelanin without disruptive sample preparation. A selenomelanin ¹³C NMR spectrum was overlaid with that of synthetic eumelanin derived from pure L-DOPA as the only monomer (Figure 1G). The peak at 163-ppm was ascribed to the COOH of selenocysteine (ssNMR of selenocystine is displayed for comparison, Figure 1G), while the decrease in the peak at 143-ppm suggests a change in the catechol group (ssNMR of L-DOPA is overlaid for comparison, Figure 1G). The catechol carbon shifted downfield could be attributed to cyclization generating the benzoselenazine functional group analogous to the benzothiazine proposed for natural pheomelanin. On the basis of this data, we argue that the adapted Raper-Mason model is applicable to the selenomelanin material (Figure S4). Attempts to obtain $^{77}\mathrm{Se}$ NMR were unsuccessful, likely due to the low mobility of selenium in the polymer and the intrinsic paramagnetic nature of selenomelanin. The integrated areas of both carbonyl peaks in the SeNP spectrum suggest the molar ratio of selenocysteine and L-DOPA to be 0.42:1(Figure S5). Inductively coupled plasma optical emission spectrometry (ICP-OES) indicated a similar molar ratio of 0.44:1, corresponding to a benzoselenazine subunit content of $\sim\!55\%$ (w/w). In addition, circular dichroism (CD) spectroscopy (Figure S6) showed that despite using two chiral starting materials, intramolecular cyclization leads to an achiral structure.

Synthesis of Pheomelanin Nanoparticles (PNPs) and Eumelanin Nanoparticles (L-DOPA NPs). PNPs were synthesized using L-cysteine and L-DOPA (Figure 2, Table 1, Figure S7) according to literature procedures. 35 PNPs have a sulfur content of \sim 7.5% as determined by ICP-OES, which is similar to that of natural pheomelanin. 17 XPS confirmed the presence of sulfur (Figure S7), yet ssNMR (Figure 2C) revealed the absence of benzothiazine groups in the final product. CD spectroscopy of PNP shows a clear signal (Figure S7) indicating a chiral structure, which is consistent with the ssNMR results and the presence of noncyclized cysteine adducts. The oxidation of L-DOPA and cysteine using tyrosinase³⁹ gave similar results to the permanganate oxidation as determined by ¹³C ssNMR spectroscopy (Figure S8). We reasoned that while the addition of cysteine occurred, the subsequent intramolecular cyclization step was hindered by

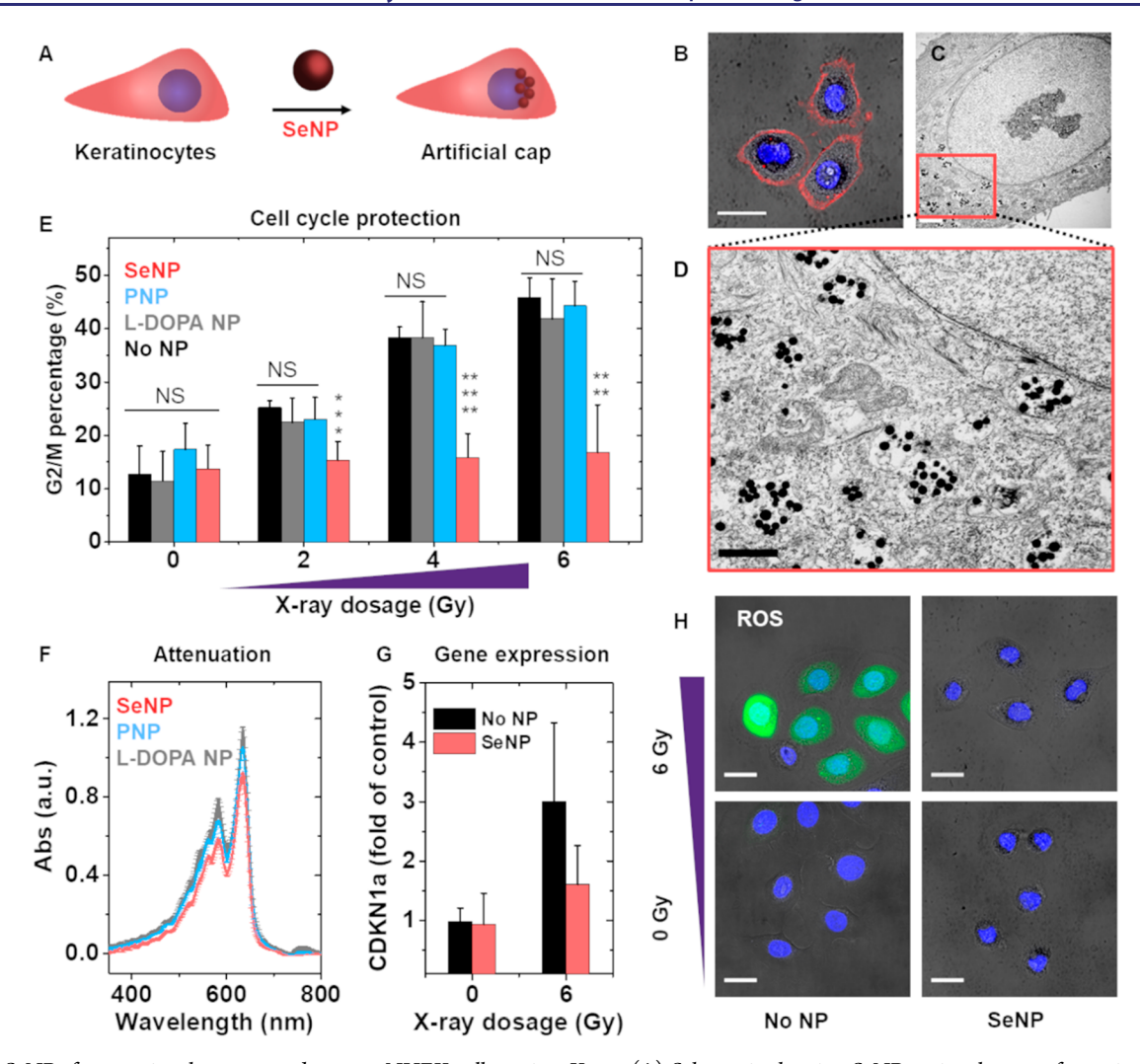


Figure 3. SeNPs form perinuclear caps and protect NHEK cells against X-ray. (A) Schematic showing SeNP perinuclear cap formation in NHEK cells. Cells treated with SeNP for 24 h, and imaged via CLSM (B, Scale bar 20 μ m), and STEM (C, scale bar 2 μ m, D, scale bar 1 μ m). For B, cells were stained with wheat germ agglutinin (WGA) (red) and Hoechst 33342 (blue). (E) SeNPs protect cells against cell cycle changes induced by X-rays. G2/M phase populations for each NP were plotted against X-ray dosage. Error bars represent standard deviation from at least three experiments. NS means no statistical difference (P > 0.01), *** $P < 10^{-3}$, **** $P < 10^{-4}$, ****** $P < 10^{-6}$, with reference to no NP control at same X-ray dose, determined by Student's two-tailed t test. (F) Attenuation of NP suspension measured by EBT3 Radiochromic film. Error bars represent standard deviation from three experiments. (G) CDKN1a gene expression level decreased by SeNP treatment. Error bars represent standard deviation from three experiments. (H) Live-cell imaging of ROS scavenging by CLSM showing DCFDA ROS-positive signal (green), and nuclei stained with Hoechst 33342 (blue). Scale bar 20 μ m.

electron-donation of the sulfide group to the quinone, whereas for selenocysteine, the weaker electron-donating capability of selenide groups results in a more electrophilic ortho quinone group due to orbital mismatch between selenium and quinone. It should be noted that, to the best of our knowledge, papers reporting the synthesis of pheomelanins have omitted ssNMR data. Here, we find that the published method in our hands results in an absence of benzothiazine rings and the presence of dangling cysteines, bringing into question how analogous this synthetic pheomelanin is to that from natural sources. Regardless, for comparison, we designate this material as a synthetic pheomelanin and utilize it in functional studies against the SeNP analogue (vide infra).35 We note that in addition to the synthetic route, and for structure verification, natural pheomelanin was extracted from the covert feathers of a Rhode Island red rooster (Figure 2D) which have high pheomelanin content.⁴¹ This natural pheomelanin has an aromatic region analogous to what we observe in the SeNP

ssNMR spectrum (Figure 2C inset), corresponding to the proposed benzothiazine structure (Figure S9).

Eumelanin control particles (L-DOPA NP) were prepared *via* oxidative polymerization of L-DOPA (Figure S10). ³⁵ The three types of melanin NPs (SeNP, PNP and L-DOPA NP) are all spherical, with similar radii and negative ζ potentials (Table 1). Their stability was investigated under various conditions, including dilution, ionic strength, and varying pH (Figures S11, S12). SeNPs showed good stability under ambient conditions, low refractive index (Figure S13), and solubility in alkaline conditions.

Cytotoxicity and Perinuclear Cap Formation. With melanin nanoparticles in hand, we explored their toxicity and subcellular distribution in NHEK cells. Our prior work has shown that polydopamine-based synthetic melanin can mimic natural eumelanin and form artificial perinuclear caps in keratinocytes which protect them against UV damage. Cytotoxicity experiments using NHEK cells (Figure S14)

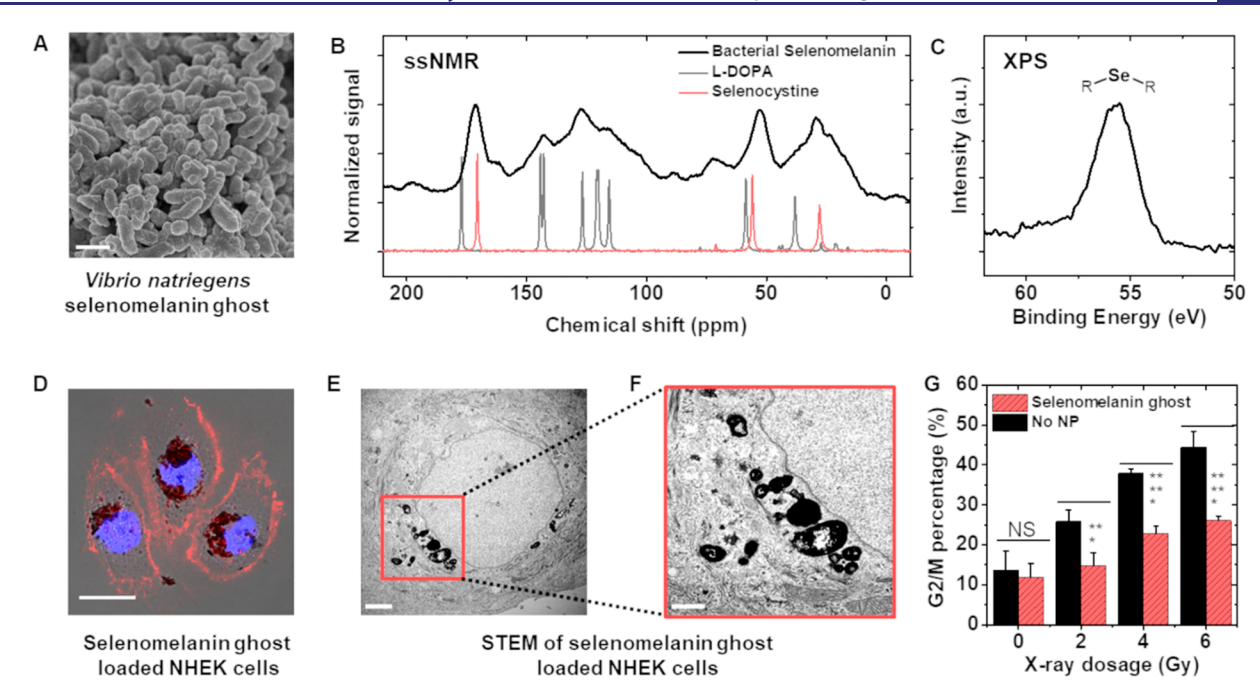


Figure 4. Radioprotecting selenomelanin synthesized by living cells. (A) SEM of selenomelanin ghosts made by V. natriegens fed with selenocystine and L-DOPA. Scale bar 1 μ m. (B) 13 C ssNMR of selenomelanin nanoparticles made by V. natriegens in culture medium. (C) XPS Se 3d spectrum of selenomelanin ghosts. (D) Representative CLSM image showing perinuclear caps in NHEK cells formed by selenomelanin ghosts. Cell membranes were stained with WGA (red), and nuclei with Hoechst 33342 (blue). Scale bar 20 μ m. (E) Representative STEM micrograph showing the perinuclear caps formed in NHEK cells. Scale bar 2 μ m. (F) Zoomed STEM image showing semihollow selenomelanin ghosts in the perinuclear region. Scale bar 1 μ m. (G) Selenomelanin ghosts protect against cell cycle arrest induced by X-rays. Error bars represent standard deviation from three experiments. NS P > 0.01, *** $P < 10^{-3}$, ***** $P < 10^{-5}$, determined by Student's two-tailed t test.

indicated that SeNP has good biocompatibility below 0.02 mg mL⁻¹, similar to L-DOPA NP. Next, the intracellular distribution was studied after incubating NHEK cells with NPs for 24 h (Figure 3). Artificial perinuclear caps were observed by confocal laser scanning microscopy (CLSM) (Figure 3A,B).

Scanning transmission electron microscopy (STEM) studies (Figure 3C,D) detected SeNPs inside vesicles in the perinuclear area of keratinocytes and dispersed in keratin filaments, suggesting the same distribution as natural melanosomes. Similar behaviors were observed for PNP and L-DOPA NPs (Figure S15, S16). Note that in this scenario, the comparison to pheomelanin is specific to the synthetic pheomelanin made by the commonly employed literature methods³⁵ and more work is needed to develop a high quality synthetic mimic for further testing.

Superior Protection Observed for SeNP against X-ray Irradiation As Compared to PNP or L-DOPA NP. We then studied the protection effects of NPs against X-ray irradiation by assaying for G2/M phase cell cycle arrest (Figure 3E). In initial studies, NHEK cell cycle distributions were determined by flow cytometry at different time points following 6-Gy X-ray irradiation. Untreated NHEK cells showed an increase from 15% to 46% in the population of cells in the G2/M phase 24 h postirradiation (Figures S17, S18); therefore, 24 h time points were used for further cell cycle studies. NHEK cells were otherwise morphologically intact 24 h following X-ray treatment (Figure S19).

Cell cycle experiments on treated cells revealed that of the three particles, only SeNP prevented G2/M arrest induced by X-rays (Figure 3E, Figure S20, Table S1). In these studies, NHEK cells were treated with one of the synthetic melanin NPs (NP concentrations were kept at 0.004 mg mL⁻¹ to

eliminate possible quenching of the propidium iodide fluorescence) and then irradiated with either 0, 2, 4, or 6 Gy of X-ray radiation. It is worth noting that a typical clinical dose used for cancer radiotherapy patients is 1.8-2 Gy per day, while 5 Gy of radiation is lethal to humans.⁴² For SeNPs, even after 6 Gy X-ray irradiation, the G2/M phase population remained at 17%, which is statistically identical to non-X-ray treated cells (P = 0.22). Another eumelanin control, namely, polydopamine nanoparticles (PDA NPs), was synthesized and utilized. Cell cycle experiments showed that after 6 Gy radiation, the G2/M phase population increased to 33% (Figure S21). This result further confirms the superior protection effect of selenomelanin. The FDA approved drug amifostine for cytoprotection against radiotherapy was also tested, yet no difference was observed compared to the control where particles were omitted (Figure S22). Moreover, the viability of cells protected by SeNPs was maintained after 6 Gy irradiation (Figures S23, S24 and Table S2). These results indicate that SeNPs can protect human skin cells from X-rayinduced cell cycle changes. While using selenomelanin for Xray protection, direct exposure to sunlight should be avoided since pheomelanin has pro-oxidant properties upon photo excitation. 19

To explore the mechanism of protection by SeNPs, we assessed the antioxidant properties of the different particles. Exposure of a living system to high energy radiation leads to the ionization of water and the subsequent production of toxic reactive oxygen species (ROS), which accounts for approximately two-thirds of the biological damage produced by X-rays. Live-cell imaging shows strong green fluorescence from the fluorogenic ROS probe (2',7'-dichlorofluorescein diacetate, DCFDA) after 6 Gy X-ray irradiation in the non-NP treated control (Figure 3H). Conversely, a very low ROS signal

was observed for NP treated groups, suggesting the efficient elimination of ROS (Figures S25, S26). A subsequent DPPH assay (2,2-diphenyl-1-(2,4,6-trinitrophenyl) hydrazyl) (Figure S27) revealed that L-DOPA NPs are faster at quenching radicals than SeNPs and PNPs. This rapid scavenging detoxifies cells with respect to ROS caused by X-ray irradiation and maintains a robust redox balance in cells.

The radiation-related gene expression level of cyclindependent kinase inhibitor, a regulator of cell cycle progression, was also assessed. Reverse transcription polymerase chain reaction (RT-PCR) studies (Figure 3G) revealed a 3fold upregulation of the cyclin-dependent kinase inhibitor 1a (CDKN1a) gene 3 h after 6 Gy X-ray radiation (P < 0.0001). SeNP treatment suppressed CDKN1a expression in NHEK cells significantly (P = 0.01). Additionally, we compared the Xray attenuation capability of the different NPs. Nanoparticle suspensions were placed over radiochromic film and exposed to X-ray radiation. The film underneath the SeNPs had the lowest absorbance at 635 nm (Figure 3F, Figure S28), while the L-DOPA NP and PNP suspensions had no statistical difference in the film absorption, suggesting that SeNPs can better attenuate X-ray radiation. Taken together, ROS scavenging, gene expression regulation, and physical attenuation all contribute to the superior protective effects of SeNPs.

Biosynthesis of selenomelanin. It is known that fungi and bacteria metabolize selenium species contributing to selenium cycling in nature. 44,45 In addition, eukaryotic species such as mammals, ancient fungi, nematodes, and Drosophila produce one or more selenoproteins. Furthermore, it was recently reported that when zebrafish larvae were treated with selenium compounds, selenium preferentially accumulated in melanized cells. 48 However, the authors did not argue that the melanin itself acted as a repository for the selenium but rather that proteins in those cells had incorporated the element. These facts lead to our reasoning that selenomelanin should be a part of the melanin family. Therefore, we set out to show whether bacteria genetically modified with a tyrosinase gene can produce selenomelanin in vitro if given selenocystine. To test this, we fed selenocystine and L-DOPA to engineered tyrosinase-producing Vibrio natriegens (Figure 4, Figure S29). Melanin was produced in cell-free supernatant as nanoparticles, or in association with the cell walls, to form micron-size melanin ghosts (Figure 4A, Figure S30). ssNMR of the nanoparticles (Figure 4B) showed similar features to those of synthetic selenomelanin (Figure 1G). FTIR spectra (Figure S31) suggested the presence of amide bonds from peptidoglycans. ICP-OES indicated the presence of selenium, while XPS (Figure 4C, Figure S32) showed increased counts of the Se 3d band with longer beam etching times, suggesting that selenomelanin is buried inside the bacterial cell wall, further affirming that selenomelanin could be naturally incorporated in live cells through biosynthetic pathways. Indeed, the successful incorporation of selenium in biosynthesized melanin provides a possible answer to the question of selenium accumulation in melanized tissues of zebrafish in previous studies. 48

We finally explored whether the biosynthesized selenomelanin could provide any X-ray protection. Light microscopy (Figure 4D) showed that selenomelanin ghosts were internalized and formed perinuclear caps in NHEK cells. STEM microscopy also supported the melanosome-mimicking distribution (Figure 4E) and the semihollow structure of the ghosts (Figure 4F). Cell cycle distribution studies showed that biosynthetic selenomelanin also decreased G2/M arrest caused by X-rays (Figure 4G, Table S3). These promising results show that selenomelanin is a feasible natural melanin and that it could be beneficial to some organisms where high selenium and high radiation exposure are found in natural ecosystems. This work points to the possibility that melanin acts as a repository for selenium and that it may be an important part of selenium metabolism.

CONCLUSIONS

In summary, selenomelanin, a new, abiotic form of melanin, was prepared. Its synthesis was achieved *via* copolymerization of the naturally occurring amino acid selenocysteine and the tyrosine oxidation product, L-DOPA. The nanoparticle form of selenomelanin, SeNPs, form perinuclear caps within human keratinocyte cells, where they scavenge ROS and protect against G2/M phase arrest caused by impinging ionizing radiation. We demonstrated that selenomelanin could be biosynthesized in live cells and that the material showed similar properties to the synthetic version. We anticipate that this line of research may guide the discovery of selenomelanin in nature where an abundant source of selenium and high radiation are both present.

ASSOCIATED CONTENT

Supporting Information

The Supporting Information is available free of charge at https://pubs.acs.org/doi/10.1021/jacs.0c05573.

Detailed experimental protocols, materials and methods, additional characterization of SeNP, PNP, NHEK cells, and selenomelanin made by *Vibrio natriegens* (PDF)

AUTHOR INFORMATION

Corresponding Authors

Matthew D. Shawkey – Evolution and Optics of Nanostructures Group, Department of Biology, The University of Ghent, 9000 Ghent, Belgium; Email: matthew.shawkey@ugent.be

Michael D. Burkart — Department of Chemistry & Biochemistry, University of California, San Diego, La Jolla, California 92093, United States of America; oorcid.org/0000-0002-4472-2254; Email: mburkart@ucsd.edu

Zheng Wang — Center for Bio/Molecular Science and Engineering, US Naval Research Laboratory, Washington, D.C. 20375, United States of America; Email: zheng.wang@ nrl.navy.mil

Nathan C. Gianneschi — Department of Chemistry and Department of Materials Science and Engineering, Department of Biomedical Engineering, Department of Pharmacology, International Institute for Nanotechnology, Simpson-Querrey Institute, Chemistry of Life Processes Institute, Lurie Cancer Center, Northwestern University, Evanston, Illinois 60208, United States of America; orcid.org/0000-0001-9945-5475; Email: nathan.gianneschi@northwestern.edu

Authors

Wei Cao — Department of Chemistry and Department of Materials Science and Engineering, Department of Biomedical Engineering, Department of Pharmacology, International Institute for Nanotechnology, Simpson-Querrey Institute, Chemistry of Life Processes Institute, Lurie Cancer Center, Northwestern University, Evanston, Illinois 60208, United States of America; orcid.org/0000-0002-5048-7991

Naneki C. McCallum — Department of Chemistry, Northwestern University, Evanston, Illinois 60208, United States of America; Ocid.org/0000-0001-9210-3493

Qing Zhe Ni – Department of Chemistry & Biochemistry, University of California, San Diego, La Jolla, California 92093, United States of America

Weiyao Li — Department of Polymer Science, The University of Akron, Akron, Ohio 44325, United States of America;
orcid.org/0000-0002-8512-295X

Hannah Boyce — Department of Chemistry, Northwestern University, Evanston, Illinois 60208, United States of America

Haochuan Mao – Department of Chemistry and Institute for Sustainability and Energy, Northwestern University, Evanston, Illinois 60208, United States of America; ⊙ orcid.org/0000-0001-8742-089X

Xuhao Zhou — Department of Chemistry, Northwestern University, Evanston, Illinois 60208, United States of America; orcid.org/0000-0002-7181-607X

Hao Sun – Department of Chemistry and Department of Materials Science and Engineering, Department of Biomedical Engineering, Department of Pharmacology, International Institute for Nanotechnology, Simpson-Querrey Institute, Chemistry of Life Processes Institute, Lurie Cancer Center, Northwestern University, Evanston, Illinois 60208, United States of America; orcid.org/0000-0001-9153-4021

Matthew P. Thompson — Department of Chemistry and Department of Materials Science and Engineering, Department of Biomedical Engineering, Department of Pharmacology, International Institute for Nanotechnology, Simpson-Querrey Institute, Chemistry of Life Processes Institute, Lurie Cancer Center, Northwestern University, Evanston, Illinois 60208, United States of America

Claudia Battistella — Department of Chemistry and Department of Materials Science and Engineering, Department of Biomedical Engineering, Department of Pharmacology, International Institute for Nanotechnology, Simpson-Querrey Institute, Chemistry of Life Processes Institute, Lurie Cancer Center, Northwestern University, Evanston, Illinois 60208, United States of America

Michael R. Wasielewski — Department of Chemistry and Institute for Sustainability and Energy, Northwestern University, Evanston, Illinois 60208, United States of America; orcid.org/0000-0003-2920-5440

Ali Dhinojwala — Department of Polymer Science, The University of Akron, Akron, Ohio 44325, United States of America; Ocid.org/0000-0002-3935-7467

Complete contact information is available at: https://pubs.acs.org/10.1021/jacs.0c05573

Author Contributions

W.C. and N.C.G. conceived the project and designed the experiments. W. C. conducted the majority of experiments. N.C.M. assisted with NHEK cell culture and obtained/analyzed STEM and SEM images. Q.Z.N. and M.D.B. designed, performed, and interpreted solid-state ¹³C NMR. W.L. and A.D. measured the refractive index of selenomelanins. H.B. performed NP stability tests for aggregation by DLS. C.B. assisted with cell culture. H.M. and M.R.W. performed EPR. H.S. obtained CD spectra. X.Z. performed and analyzed radical scavenging experiments. M.D.S. obtained samples and developed methodologies for extraction of the natural pheomelanin samples. Z.W. performed biosynthesis with V.

natriegens. W.C., M.P.T., and N.C.G. cowrote the manuscript with contributions from all authors. All authors discussed and interpreted the results and revised the manuscript.

Funding

The work was supported by the Air Force Office of Scientific Research through a MURI Grant (FA9550-18-1-0142), and supplemental grant (AFOSR FA9550-18-1-0477) and FWO grant G007117N by the Assistant Secretary of Defense for Research and Engineering (ASD (R&E)) through the Applied Research for Advancement of S&T Priorities Synthetic Biology for Military Environments program which supports Z. W. EPR spectroscopy was supported by the National Science Foundation under Award NO. CHE-1900422 (M.R.W.). H. B. was supported primarily by the National Science Foundation under NSF Award Number EEC-1757618.

Notes

The authors declare the following competing financial interest(s): N. C. G. and W. C. have filed a provisional patent US 62/928,129 and are listed as inventors for selenium-containing analogues of pheomelanin, related materials, and synthetic methods.

ACKNOWLEDGMENTS

The authors thank Paul Mehl in the Flow Cytometry Core facility at Northwestern University. We thank Matthew Clutter at the Center for Molecular Innovation and Drug Discovery at Northwestern University for helpful discussions in the design of X-ray radiation experiments. The authors acknowledge the aid of Prof. Bethany Perez-White in the department of dermatology at Northwestern Feinberg School of Medicine for providing NHEK cells and for lending her expertise in keratinocyte cell culture. We thank Prof. Dimitre H. Hristov in the Department of Radiation Oncology, Stanford University for help in the design of radiation experiments and Prof Vythialingam Sathiaseelan at Northwestern Feinberg School of Medicine for providing us with X-ray film. Finally, we thank Sara Fernandez Dunne at Northwestern's High Throughput Analysis Core for her assistance with conducting RT-PCR experiments. We would also like to thank Northwestern NUANCE BioCryo staff scientists Eric W. Roth and Charlene Wilke for their assistance in TEM cell embedding and microtomy.

ABBREVIATIONS

SeNP, selenomelanin nanoparticle; NP, nanoparticle; Sec, selenocysteine; SECIS, SElenoCysteine Insertion Sequence; L-DOPA, L-3,4-dihydroxyphenylalanine; EPR, electron paramagnetic resonance; XPS, X-ray photoelectron spectroscopy; NHEK, neonatal human epidermal keratinocytes; PDA NP, polydopamine nanoparticle; TEM, transmission electron microscopy; FTIR, Fourier-transform infrared spectroscopy; ROS, reactive oxygen species; HPLC, high performance liquid chromatography; ICP-OES, inductively coupled plasma optical emission spectrometry; ssNMR, solid-state nuclear magnetic resonance; PNPs, Pheomelanin nanoparticles; CLSM, confocal laser scanning microscopy; STEM, Scanning transmission electron microscopy; WGA, wheat germ agglutinin; DCFDA, 2',7'-dichlorofluorescein diacetate; DPPH, 2,2-diphenyl-1-(2,4,6-trinitrophenyl) hydrazyl; RT-PCR, reverse transcription polymerase chain reaction; CDKN1a, cyclin-dependent kinase inhibitor 1a

REFERENCES

- (1) D'Alba, L.; Shawkey, M. D. Melanosomes: Biogenesis, Properties, and Evolution of an Ancient Organelle. *Physiol. Rev.* **2019**, 99 (1), 1–19.
- (2) d'Ischia, M.; Napolitano, A.; Ball, V.; Chen, C. T.; Buehler, M. J. Polydopamine and eumelanin: from structure-property relationships to a unified tailoring strategy. *Acc. Chem. Res.* **2014**, *47* (12), 3541–50.
- (3) Lampel, A.; McPhee, S. A.; Park, H.-A.; Scott, G. G.; Humagain, S.; Hekstra, D. R.; Yoo, B.; Frederix, P. W. J. M.; Li, T.-D.; Abzalimov, R. R.; Greenbaum, S. G.; Tuttle, T.; Hu, C.; Bettinger, C. J.; Ulijn, R. V. Polymeric peptide pigments with sequence-encoded properties. *Science* **2017**, 356 (6342), 1064–1068.
- (4) Glass, K.; Ito, S.; Wilby, P. R.; Sota, T.; Nakamura, A.; Bowers, C. R.; Vinther, J.; Dutta, S.; Summons, R.; Briggs, D. E.; Wakamatsu, K.; Simon, J. D. Direct chemical evidence for eumelanin pigment from the Jurassic period. *Proc. Natl. Acad. Sci. U. S. A.* **2012**, *109* (26), 10218–23.
- (5) Wang, C.; Wang, D.; Dai, T.; Xu, P.; Wu, P.; Zou, Y.; Yang, P.; Hu, J.; Li, Y.; Cheng, Y. Skin Pigmentation-Inspired Polydopamine Sunscreens. *Adv. Funct. Mater.* **2018**, 28 (33), 1802127.
- (6) Maia, R.; Rubenstein, D. R.; Shawkey, M. D. Key ornamental innovations facilitate diversification in an avian radiation. *Proc. Natl. Acad. Sci. U. S. A.* **2013**, *110* (26), 10687–10692.
- (7) Xiao, M.; Li, Y.; Allen, M. C.; Deheyn, D. D.; Yue, X.; Zhao, J.; Gianneschi, N. C.; Shawkey, M. D.; Dhinojwala, A. Bio-Inspired Structural Colors Produced *via* Self-Assembly of Synthetic Melanin Nanoparticles. *ACS Nano* **2015**, *9* (5), 5454–5460.
- (8) Lee, H.; Dellatore, S. M.; Miller, W. M.; Messersmith, P. B. Mussel-Inspired Surface Chemistry for Multifunctional Coatings. *Science* **2007**, 318 (5849), 426–430.
- (9) Lee, H.; Lee, B. P.; Messersmith, P. B. A reversible wet/dry adhesive inspired by mussels and geckos. *Nature* **2007**, *448* (7151), 338–41.
- (10) Panzella, L.; Gentile, G.; D'Errico, G.; Della Vecchia, N. F.; Errico, M. E.; Napolitano, A.; Carfagna, C.; d'Ischia, M. Atypical structural and pi-electron features of a melanin polymer that lead to superior free-radical-scavenging properties. *Angew. Chem., Int. Ed.* **2013**, 52 (48), 12684–7.
- (11) Seagle, B.-L. L.; Rezai, K. A.; Kobori, Y.; Gasyna, E. M.; Rezaei, K. A.; Norris, J. R., Jr. Melanin photoprotection in the human retinal pigment epithelium and its correlation with light-induced cell apoptosis. *Proc. Natl. Acad. Sci. U. S. A.* **2005**, *102* (25), 8978–8983.
- (12) Liu, Y.; Ai, K.; Ji, X.; Askhatova, D.; Du, R.; Lu, L.; Shi, J. Comprehensive Insights into the Multi-Antioxidative Mechanisms of Melanin Nanoparticles and Their Application To Protect Brain from Injury in Ischemic Stroke. *J. Am. Chem. Soc.* 2017, 139 (2), 856–862.
- (13) Seagle, B.-L. L.; Rezai, K. A.; Gasyna, E. M.; Kobori, Y.; Rezaei, K. A.; Norris, J. R. Time-Resolved Detection of Melanin Free Radicals Quenching Reactive Oxygen Species. *J. Am. Chem. Soc.* **2005**, *127* (32), 11220–11221.
- (14) Simon, J. D.; Peles, D. N. The Red and the Black. Acc. Chem. Res. 2010, 43 (11), 1452–1460.
- (15) Sealy, R.; Hyde, J.; Felix, C.; Menon, I.; Prota, G. Eumelanins and pheomelanins: characterization by electron spin resonance spectroscopy. *Science* **1982**, 217 (4559), 545–547.
- (16) Napolitano, A.; Panzella, L.; Leone, L.; d'Ischia, M. Red Hair Benzothiazines and Benzothiazoles: Mutation-Inspired Chemistry in the Quest for Functionality. *Acc. Chem. Res.* **2013**, *46* (2), 519–528.
- (17) Ito, S.; Novellino, E.; Chioccara, F.; Misuraca, G.; Prota, G. Copolymerization of dopa and cysteinyldopa in melanogenesis *in vitro*. *Experientia* **1980**, *36* (7), 822–3.
- (18) Premi, S.; Wallisch, S.; Mano, C. M.; Weiner, A. B.; Bacchiocchi, A.; Wakamatsu, K.; Bechara, E. J. H.; Halaban, R.; Douki, T.; Brash, D. E. Chemiexcitation of melanin derivatives induces DNA photoproducts long after UV exposure. *Science* **2015**, 347 (6224), 842–847.

- (19) Solano, F. Photoprotection *versus* photodamage: updating an old but still unsolved controversy about melanin. *Polym. Int.* **2016**, *65* (11), 1276–1287.
- (20) Schweitzer, A. D.; Howell, R. C.; Jiang, Z.; Bryan, R. A.; Gerfen, G.; Chen, C.-C.; Mah, D.; Cahill, S.; Casadevall, A.; Dadachova, E. Physico-Chemical Evaluation of Rationally Designed Melanins as Novel Nature-Inspired Radioprotectors. *PLoS One* **2009**, 4 (9), No. e7229.
- (21) Sinilova, N. G.; Pershina, Z. G.; Duplitseva, A. P.; Pavlova, I. B. A radio-resistant pigmented bacterial culture isolated from atomic reactor water. *Zh Mikrobiol Epidemiol Immunobiol* **1969**, 46 (8), 94–9.
- (22) Mironenko, N. V.; Alekhina, I. A.; Zhdanova, N. N.; Bulat, S. A. Intraspecific variation in gamma-radiation resistance and genomic structure in the filamentous fungus Alternaria alternata: a case study of strains inhabiting Chernobyl reactor no. 4. *Ecotoxicol. Environ. Saf.* **2000**, 45 (2), 177–87.
- (23) Dadachova, E.; Casadevall, A. Ionizing radiation: how fungi cope, adapt, and exploit with the help of melanin. *Curr. Opin. Microbiol.* **2008**, *11* (6), 525–31.
- (24) Thureau, P.; Ziarelli, F.; Thevand, A.; Martin, R. W.; Farmer, P. J.; Viel, S.; Mollica, G. Probing the motional behavior of eumelanin and pheomelanin with solid-state NMR spectroscopy: new insights into the pigment properties. *Chem. Eur. J.* **2012**, *18* (34), 10689–700.
- (25) Durante, M.; Cucinotta, F. A. Physical basis of radiation protection in space travel. *Rev. Mod. Phys.* **2011**, 83 (4), 1245–1281.
- (26) Hasegawa, A.; Tanigawa, K.; Ohtsuru, A.; Yabe, H.; Maeda, M.; Shigemura, J.; Ohira, T.; Tominaga, T.; Akashi, M.; Hirohashi, N.; Ishikawa, T.; Kamiya, K.; Shibuya, K.; Yamashita, S.; Chhem, R. K. Health effects of radiation and other health problems in the aftermath of nuclear accidents, with an emphasis on Fukushima. *Lancet* **2015**, 386 (9992), 479–488.
- (27) Shimazu, F.; Tappel, A. L. Selenoamino Acids: Decrease of Radiation Damage to Amino Acids and Proteins. *Science* **1964**, *143* (3604), 369–371.
- (28) Kunwar, A.; Bag, P. P.; Chattopadhyay, S.; Jain, V. K.; Priyadarsini, K. I. Anti-apoptotic, anti-inflammatory, and immuno-modulatory activities of 3,3'-diselenodipropionic acid in mice exposed to whole body gamma-radiation. *Arch. Toxicol.* **2011**, 85 (11), 1395–405
- (29) Xu, H.; Cao, W.; Zhang, X. Selenium-Containing Polymers: Promising Biomaterials for Controlled Release and Enzyme Mimics. *Acc. Chem. Res.* **2013**, *46* (7), 1647–1658.
- (30) Kryukov, G. V.; Castellano, S.; Novoselov, S. V.; Lobanov, A. V.; Zehtab, O.; Guigo, R.; Gladyshev, V. N. Characterization of mammalian selenoproteomes. *Science* **2003**, *300* (5624), 1439–43.
- (31) Ursini, F.; Heim, S.; Kiess, M.; Maiorino, M.; Roveri, A.; Wissing, J.; Flohé, L. Dual Function of the Selenoprotein PHGPx During Sperm Maturation. *Science* **1999**, 285 (5432), 1393–1396.
- (32) Shisler, J. L.; Senkevich, T. G.; Berry, M. J.; Moss, B. Ultraviolet-Induced Cell Death Blocked by a Selenoprotein from a Human Dermatotropic Poxvirus. *Science* **1998**, 279 (5347), 102–105.
- (33) Ji, S.; Cao, W.; Yu, Y.; Xu, H. Dynamic diselenide bonds: exchange reaction induced by visible light without catalysis. *Angew. Chem., Int. Ed.* **2014**, 53 (26), 6781–5.
- (34) Lusic, H.; Grinstaff, M. W. X-ray-computed tomography contrast agents. *Chem. Rev.* **2013**, *113* (3), 1641–1666.
- (35) Pyo, J.; Ju, K. Y.; Lee, J. K. Artificial pheomelanin nanoparticles and their photo-sensitization properties. *J. Photochem. Photobiol., B* **2016**, *160*, 330–5.
- (36) Zhou, X.; McCallum, N. C.; Hu, Z.; Cao, W.; Gnanasekaran, K.; Feng, Y.; Stoddart, J. F.; Wang, Z.; Gianneschi, N. C. Artificial Allomelanin Nanoparticles. ACS Nano 2019, 13 (10), 10980–10990.
- (37) Schweitzer, A. D.; Howell, R. C.; Jiang, Z.; Bryan, R. A.; Gerfen, G.; Chen, C. C.; Mah, D.; Cahill, S.; Casadevall, A.; Dadachova, E. Physico-chemical evaluation of rationally designed melanins as novel nature-inspired radioprotectors. *PLoS One* **2009**, *4* (9), No. e7229.

- (38) Ito, S.; Fujita, K. Microanalysis of eumelanin and pheomelanin in hair and melanomas by chemical degradation and liquid chromatography. *Anal. Biochem.* **1985**, *144* (2), 527–536.
- (39) Ito, S. Optimization of conditions for preparing synthetic pheomelanin. *Pigm. Cell Res.* **1989**, 2 (1), 53–6.
- (40) Huang, Y.; Li, Y.; Hu, Z.; Yue, X.; Proetto, M. T.; Jones, Y.; Gianneschi, N. C. Mimicking Melanosomes: Polydopamine Nanoparticles as Artificial Microparasols. *ACS Cent. Sci.* **2017**, 3 (6), 564–569.
- (41) Smyth, J. R., Jr.; Porter, J. W.; Bohren, B. B. A study of pigments from red, brown, and buff feathers and hair. *Physiol. Zool.* **1951**, 24 (3), 205–16.
- (42) Dadachova, E.; Bryan, R. A.; Howell, R. C.; Schweitzer, A. D.; Aisen, P.; Nosanchuk, J. D.; Casadevall, A. The radioprotective properties of fungal melanin are a function of its chemical composition, stable radical presence and spatial arrangement. *Pigm. Cell Melanoma Res.* **2008**, 21 (2), 192–9.
- (43) National Research Council, S.; Committee on the Biological Effects of Ionizing, R., Health Effects of Exposure to Low Levels of Ionizing Radiation: BEIR V. 2001.
- (44) Fernandez-Llamosas, H.; Castro, L.; Blazquez, M. L.; Diaz, E.; Carmona, M. Speeding up bioproduction of selenium nanoparticles by using *Vibrio natriegens* as microbial factory. *Sci. Rep.* **2017**, *7* (1), 16046.
- (45) Rosenfeld, C. E.; Kenyon, J. A.; James, B. R.; Santelli, C. M. Selenium (IV,VI) reduction and tolerance by fungi in an oxic environment. *Geobiology* **2017**, *15* (3), 441–452.
- (46) Mariotti, M.; Salinas, G.; Gabaldon, T.; Gladyshev, V. N. Utilization of selenocysteine in early-branching fungal phyla. *Nat. Microbiol* **2019**, 4 (5), 759–765.
- (47) Schomburg, L.; Schweizer, U.; Köhrle, J. Selenium and selenoproteins in mammals: extraordinary, essential, enigmatic. *Cell. Mol. Life Sci.* **2004**, *61* (16), 1988–1995.
- (48) Dolgova, N. V.; Hackett, M. J.; MacDonald, T. C.; Nehzati, S.; James, A. K.; Krone, P. H.; George, G. N.; Pickering, I. J. Distribution of selenium in zebrafish larvae after exposure to organic and inorganic selenium forms. *Metallomics* **2016**, *8* (3), 305–12.
- (49) Wang, Z.; Tschirhart, T.; Schultzhaus, Z.; Kelly, E. E.; Chen, A.; Oh, E.; Nag, O.; Glaser, E. R.; Kim, E.; Lloyd, P. F.; Charles, P. T.; Li, W.; Leary, D.; Compton, J.; Phillips, D. A.; Dhinojwala, A.; Payne, G. F.; Vora, G. J. Characterization and application of melanin produced by the fast-growing marine bacterium *Vibrio natriegens* through heterologous biosynthesis. *Appl. Environ. Microbiol.* **2020**, 2749 DOI: 10.1128/AEM.02749-19.